Forcing and response in simulated 20th and 21st century surface energy and precipitation trends

Timothy Andrews[1]

Received 13 January 2009; revised 11 June 2009; accepted 17 June 2009; published 11 September 2009.

[1] A simple methodology is applied to a transient integration of the Met Office Hadley Centre Global Environmental Model version1 (UKMO-HadGEM1) fully coupled atmosphere-ocean general circulation model in order to separate forcing from climate response in simulated 20th century and future global mean surface energy and precipitation trends. Forcings include any fast responses that are caused by the forcing agent and that are independent of global temperature change. Results reveal that surface radiative forcing is dominated by shortwave forcing over the 20th and 21st centuries, which is strongly negative. However, when fast responses of surface turbulent heat fluxes are separated from climate feedbacks, and included in the forcing, net surface forcing becomes positive. The nonradiative forcings are the result of rapid surface and tropospheric adjustments and impact 20th century, as well as future, evaporation and precipitation trends. A comparison of energy balance changes in eight different climate models finds that all models exhibit a positive surface energy imbalance by the late 20th century. However, there is considerable disagreement in how this imbalance is partitioned between the longwave, shortwave, latent heat and sensible heat fluxes. In particular, all models show reductions in shortwave radiation absorbed at the surface by the late 20th century compared to the pre-industrial control state, but the spread of this reduction leads to differences in the sign of their latent heat flux changes and thus in the sign of their hydrological responses.

Citation: Andrews, T. (2009), Forcing and response in simulated 20th and 21st century surface energy and precipitation trends, *J. Geophys. Res.*, *114*, D17110, doi:10.1029/2009JD011749.

1. Introduction

[2] Climate change is often understood in the context of forcing and response [e.g., *Forster et al.*, 2007]. Forcing and response are usually quantified from top-of-atmosphere (TOA) or tropopause radiation fluxes [e.g., *Forster et al.*, 2007; *Randall et al.*, 2007]; more recently the importance of understanding surface energy fluxes has been highlighted [e.g., *National Research Council*, 2005; *Andrews et al.*, 2009]. Understanding how climate change mechanisms impact the surface energy balance is not only useful for interpreting surface-air-temperature change (ΔT) but also hydrological cycle changes [e.g., *Boer*, 1993; *Allen and Ingram*, 2002; *Wild et al.*, 2008].

[3] During transient climate change the energy imbalance gives a measure of combined forcing and response. Over the global ocean an imbalance of energy at the surface is closely related to changes in ocean heat content. As the oceans are the dominant reservoir for excess heat in the climate system [e.g., *Levitus et al.*, 2005] it is often assumed that changes in ocean heat content match the Earth's planetary energy imbalance (the net absorption of radiation at the TOA by the climate system) [e.g., *Pielke*, 2003, *Hansen et al.*, 2005a]. Changes in ocean heat content, the surface energy imbalance and the TOA planetary energy imbalance provide independent checks on each other, though their relationships can be quite complex [*Zhang et al.*, 2007]. These quantities are useful because they measure the extent to which the climate is out of energy balance, and so whether any future climate change can be expected. This is different to the reporting of radiative forcings [e.g., *Forster et al.*, 2007] because radiative forcings in isolation give no indication of how much any climate response has reduced the energy imbalance caused by the forcing, and therefore, how much can be expected in the future.

[4] Recent studies have developed a paradigm whereby forcings includes fast tropospheric adjustments to the climate system [e.g., *Forster and Taylor*, 2006; *Gregory and Webb*, 2008; *Andrews and Forster*, 2008; *Williams et al.*, 2008]. These adjustments can be separated from the response to ΔT in idealized transient climate change integrations because the latter occurs predominantly over time scales determined by the heat capacity of the ocean (years or decades when considering only the mixed layer of the ocean), whereas the fast adjustment is much quicker (days or months) [*Gregory et al.*, 2004; *Gregory and Webb*, 2008]. As an adjustment to increased CO_2 levels, climate models indicate that global mean surface latent heat flux and precipitation rate rapidly reduces [e.g., *Mitchell*, 1983;

[1]School of Earth and Environment, University of Leeds, Leeds, UK.

0148-0227/09/2009JD011749

Table 1. Change in UKMO-HadGEM1 Global Mean Surface Energy Fluxes and Surface Air Temperature Averaged Over the Last 25 Years of the 20th Century and 21st Century, Under the A1B Emissions Scenario, Compared to the Pre-industrial Control State[a]

	Global Mean Change					
	Net Change		Forcing (F_i)		Response ($-\alpha_i \Delta T$)	
	1975–1999	2075–2099	1975–1999	2075–2099	1975–1999	2075–2099
LW (W m^{-2})	1.89	6.12	1.57	3.90	0.32	2.21
SW (W m^{-2})	−3.10	−4.66	−3.30	−6.07	0.20	1.41
LH (W m^{-2})	0.70	−1.87	1.67	4.85	−0.97	−6.71
SH (W m^{-2})	0.71	1.86	0.57	0.88	0.14	0.98
Net (W m^{-2})	0.20	1.46	0.51	3.60	−0.31	−2.14
Surface air temperature (K)	0.51	3.51				

[a]Also shown is the separation of the energy terms into forcing and response (see section 3). All fluxes are defined as positive downward.

Mitchell et al., 1987; *Allen and Ingram*, 2002; *Yang et al.*, 2003; *Lambert and Faull*, 2007; *Andrews et al.*, 2009] before increasing with positive ΔT. The short time scale adjustment is sufficiently large (on the order 2 W m^{-2} for surface latent heat flux in response to idealized 2 × CO_2 climate model experiments) to suggest it may be important in understanding trends of past and future surface energy and hydrological cycle changes [*Andrews et al.*, 2009], a subject of this paper.

[5] Globally averaged hydrological cycle changes may not be so relevant to climate impact studies, as regional hydrological changes can be significantly larger and of opposite sign to the global response [e.g., *Meehl et al.*, 2007]. Nevertheless, globally averaged observations exist [e.g., *Wentz et al.*, 2007; *Adler et al.*, 2008] and some suggest that climate models underestimate the global precipitation response to global warming [*Wentz et al.*, 2007]. Furthermore, the global hydrological cycle is a useful quantity to compare against the expectations of the Clausius-Clapeyron relation [*Held and Soden*, 2006].

[6] *Forster and Taylor* [2006] proposed a simple method (see section 3.1) for calculating a global mean TOA climate forcing time series from transient integrations of coupled atmosphere-ocean general circulation models (AOGCMs). In this paper I employ and validate an analogous methodology applied to global mean surface energy fluxes and precipitation rate. The methodology allows the separation of forcing-dependent adjustments from changes that occur as a response to ΔT. I apply it to one ensemble member of the Met Office Hadley Centre Global Environmental Model version 1 (UKMO-HadGEM1) simulation of the 20th century and a projection of the 21st century, under the Special Report on Emissions Scenarios (SRES) A1B scenario [*Nakicenovic and Swart*, 2000].

[7] Section 2 describes the model data and net change to the Earth's surface energy budget. Section 3 isolates the extent to which these net global mean changes are the direct result of climate forcing agents and those that result from the response to ΔT. Section 4 assesses what these results mean for interpreting modeled and observed global hydrological cycle changes. Section 5 compares the change in surface energy balance across different climate models and section 6 presents conclusions.

2. Surface Energy Budget Changes

[8] Climate model data was taken from the World Climate Research Program's (WCRP) Coupled Model Intercomparison Project phase 3 (CMIP3) multimodel data set. This large database archives the 1% yr^{-1} CO_2 increase integrations, the 20th century integrations, the SRES A1B integrations (which begin at the end of the 20th century integrations) and the pre-industrial control integrations for many AOGCMs. Here the results of UKMO-HadGEM1 are focused on. The UKMO-HadGEM1 20th century simulation ("run 2") includes the following forcings: well-mixed greenhouse gases (GHGs), tropospheric and stratospheric ozone, sulfate aerosol direct effects, sulfate aerosol indirect effects, black carbon, organic carbon, land use change, solar irradiance and volcanic aerosols [see, e.g., *Stott et al.*, 2006] (the online model documentation: http://www-pcmdi.llnl.gov/ipcc/model_documentation/ipcc_model_documentation.php).

[9] For each simulation, surface air temperature, surface energy budget terms and precipitation rate were extracted; surface energy budget terms available were downwelling/upwelling longwave (LW) and shortwave (SW) radiative fluxes, and latent heat (LH) and sensible heat (SH) non-radiative fluxes. All fluxes are then defined as positive downward, so a positive change in any surface energy term represents an energy gain at the surface. For example a positive change in the surface LH flux would indicate a reduction in the LH flux to the atmosphere and so a gain of energy at the surface. All global differences represent forced integration minus corresponding linear fits of the pre-industrial control integration. Using linear fits removes unforced model drift and reduces the overall variance as the control noise is not included in the result.

[10] Table 1 (net change columns) shows the global mean change of these variables since pre-industrial (1860) at the end of the 20th and 21st centuries. LW and SW radiation fluxes exhibit the largest changes, and are of opposite sign. By the end of the 20th century both the SH and LH fluxes to the atmosphere have been reduced. However, for the LH flux this trend reverses, so at the end of the 21st century the LH flux from the surface to the atmosphere significantly increases (change ~ -1.9 W m^{-2}) compared to the pre-industrial control state.

[11] The geographic patterns of the A1B changes are shown in Figure 1. Positive increases in surface net LW radiation are largest in the tropics. *Allan* [2006] showed changes in column integrated water vapor to be important for the net surface LW radiation budget, and these LW changes coincide with the largest increases in column atmospheric water vapor (not shown). Net surface SW radiation (Figure 1b) has been separated into clear sky

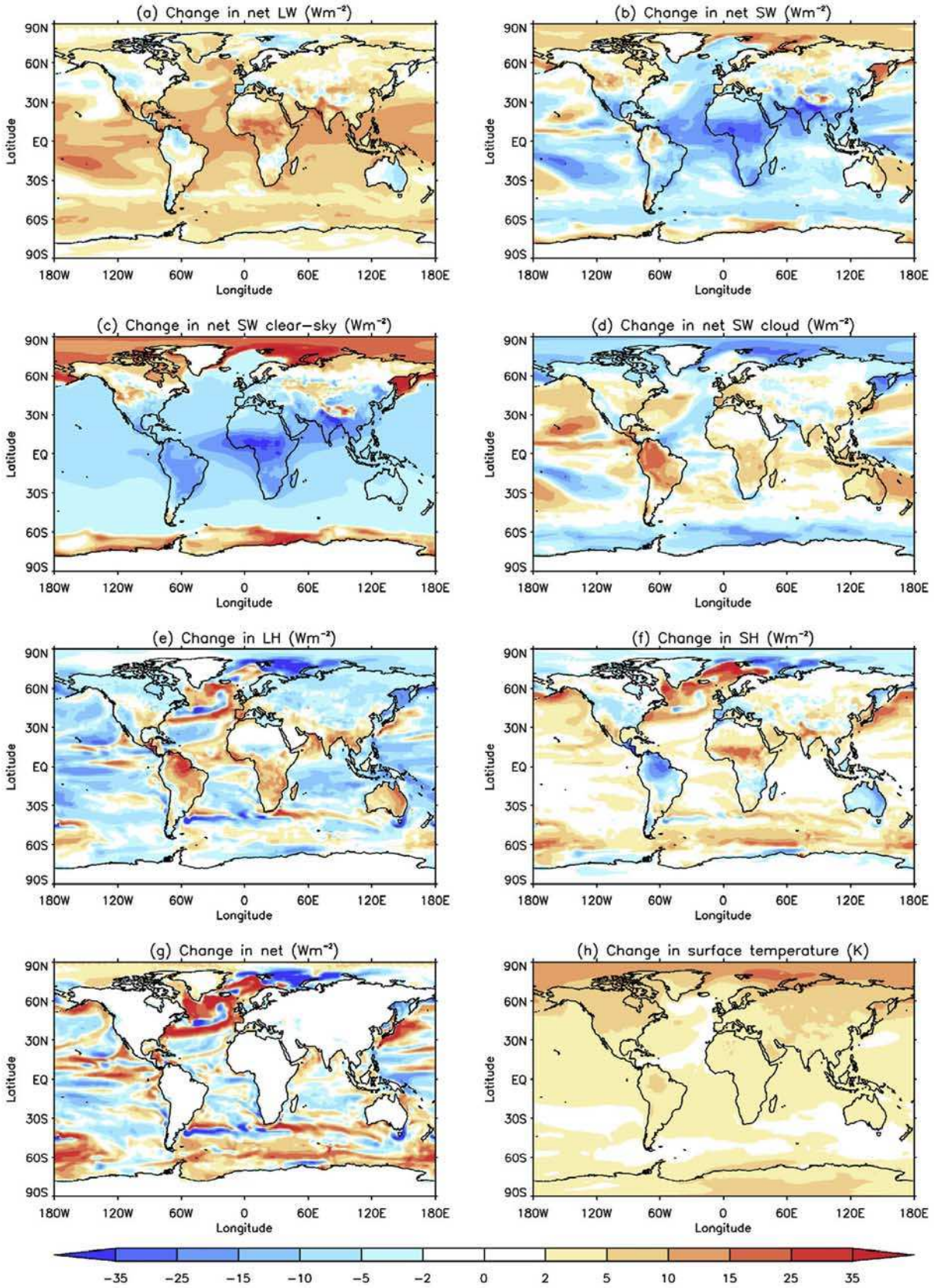

Figure 1. Change in balance of (a–g) surface energy components and (h) surface air temperature averaged over 2075–2099 of the A1B UKMO-HadGEM1 21st century simulation with respect to the pre-industrial control state. All fluxes are defined as positive downward.

(Figure 1c) and cloudy sky (Figure 1d), where changes due to clouds are calculated from all-sky fluxes minus clear-sky fluxes. Clear-sky SW (Figure 1c) changes are predominantly negative and are largest over central Africa. This region is affected by significant biomass burning aerosol that is transported into the Atlantic by the easterly trade winds. This aerosol both absorbs and scatters SW radiation (both of which will reduce SW radiation reaching the surface). Large positive SW clear-sky changes occur over regions affected by sea ice and high latitude and/or mountainous land areas. Owing to large increases in temperature in these regions (Figure 1h) surface albedo is reduced because sea ice and land snow cover retract, leading to enhanced SW surface absorption (Figure 1c). The large apparent cloud effect over these regions (Figure 1d) is most likely the result of cloud masking rather than a change in cloud properties [e.g., *Soden et al.*, 2004], because clouds shield the impact of changes in surface albedo [*Soden et al.*, 2008].

[12] LH transfer to the atmosphere increases (indicated by a negative change in Figure 1e) over most of the globe, except southern hemisphere land areas, where significant reductions occur (Figure 1e). SH flux change shows a significant land/sea contrast (Figure 1f), with most of the changes over the ocean being positive (i.e., a reduction in SH transfer to the atmosphere). Over the ocean both the turbulent heat fluxes exhibit significant changes over regions strongly influenced by ocean currents, such as the Gulf Stream and the Kuroshio and its extension off Japan (Figures 1e and 1f), where the climatological state of these fluxes are large [e.g., *Yu and Weller*, 2007]. Change in net surface heat flux (sum of LW, SW, LH and SH) is almost entirely confined to the oceans (Figure 1g), as land areas have a relatively small heat capacity and so are generally close to energy balance [*Andrews et al.*, 2009]. Over the oceans the local net surface heat flux need not be zero because (1) any imposed heating of the surface (i.e., surface forcing) cannot be quickly eliminated owing to the relatively large heat capacity of the ocean and (2) energy can be transported from one region to another by ocean currents.

3. Forcing-Dependent Changes and Climate Response

[13] To gain further insights into how the Earth's surface energy budget has changed over time it is useful to ask the following question: to what extent are changes in the Earth's surface energy budget a direct result of climate forcing agents, and how much change can be associated with longer-term climate response (i.e., the result of changes in temperature)? This is a useful question for not only improving our understanding of climate change processes but because, as I will show, a correct separation of forcing and response is important for correctly predicting time-dependent climate change [see also *Gregory and Webb*, 2008; *Williams et al.*, 2008].

3.1. Approach

[14] *Gregory et al.* [2004], *Forster and Taylor* [2006] and *Gregory and Webb* [2008] provided a simple framework for diagnosing climate forcing and feedback, as well as its separation into component form (e.g., LW and SW radiation). *Andrews et al.*] showed that an analogous framework for surface energy fluxes was robust across slab-ocean GCMs forced by $2 \times CO_2$, so that

$$N_i = F_i - \alpha_i \Delta T, \quad (1)$$

where N is the surface energy imbalance, F is the surface climate forcing, α is the surface feedback parameter and i denotes the components of the surface energy budget: LW, SW, LH and SH. Conceptually, equation (1) represents an energy balance at the Earth's surface, so that at any time, t, the surface energy imbalance, N, is equal to the additional energy flux caused by the presence of forcing agents, F, minus the energy flux generated by the climate response, $\alpha\Delta T$. If F is constant then it is equal to N in the limit of $\Delta T \rightarrow 0$, and so suggests a general definition of forcing: F is the net energy flux into the system (in this case the surface) that comes about owing to the forcing agent but before any climate response has occurred, measured by ΔT [e.g., *Shine et al.*, 2003; *Gregory et al.*, 2004; *Hansen et al.*, 2005b; *Gregory and Webb*, 2008; *Andrews and Forster*, 2008]. Using this definition of F includes any rapid adjustments that occur quicker than ΔT, such as stratospheric adjustment, the indirect and semidirect effect of aerosols, and any other analogous tropospheric adjustments.

[15] N_i and ΔT can be computed from any transient climate change simulation by simply differencing the forced and corresponding control run. If the surface feedback parameters, α_i, can be determined, then given N_i and ΔT one can calculate the time series of the surface forcing according to equation (1), and so give a complete description of the time-dependent surface energy balance.

[16] Here α_i is directly determined from the AOGCM by regressing N_i against ΔT after the 70th year in the 1% yr^{-1} CO_2 increase, until $2 \times CO_2$ is reached, experiment, at which point F_i becomes constant and so α_i can be determined from the gradient of the regression line according to equation (1) (Figures 2a and 2b). Note that *Williams et al.* [2008] performed a similar analysis for TOA radiation fluxes. This is a slightly different method to that of *Forster and Taylor* [2006], who first estimated the TOA radiative forcing for the 1% yr^{-1} CO_2 increase and then regressed TOA $N - F$ against ΔT for the first 70 years. Figures 2a and 2b show that all components follow straight lines and therefore support the linear analysis, so regression of N_i against ΔT after 70 years is sufficient to confidently determine α_i and avoids the need to estimate the forcing.

[17] Table 2 shows the diagnosed surface feedback parameters from the gradients of the regression lines in Figures 2a and 2b, note that from now on the reported feedback parameters are defined as $Y_i = -\alpha_i$ as this suits its physical interpretation better [e.g., *Gregory and Webb*, 2008], so a positive Y_i represents a positive surface feedback on climate change. The qualitative features described by *Andrews et al.* [2009], who calculated the Y_i components for many slab-ocean GCMs, are also shown in the fully coupled AOGCM, for example, positive LW and SH feedbacks and stability achieved by a strong negative LH feedback [see also, e.g., *Ramanathan*, 1981; *Gregory and Webb*, 2008]. A positive surface SW feedback is also found in UKMO-HadGEM1, but this response is uncertain across models [*Andrews et al.*, 2009]. There is, however, significant differences in the feedback strengths between UKMO-HadGEM1

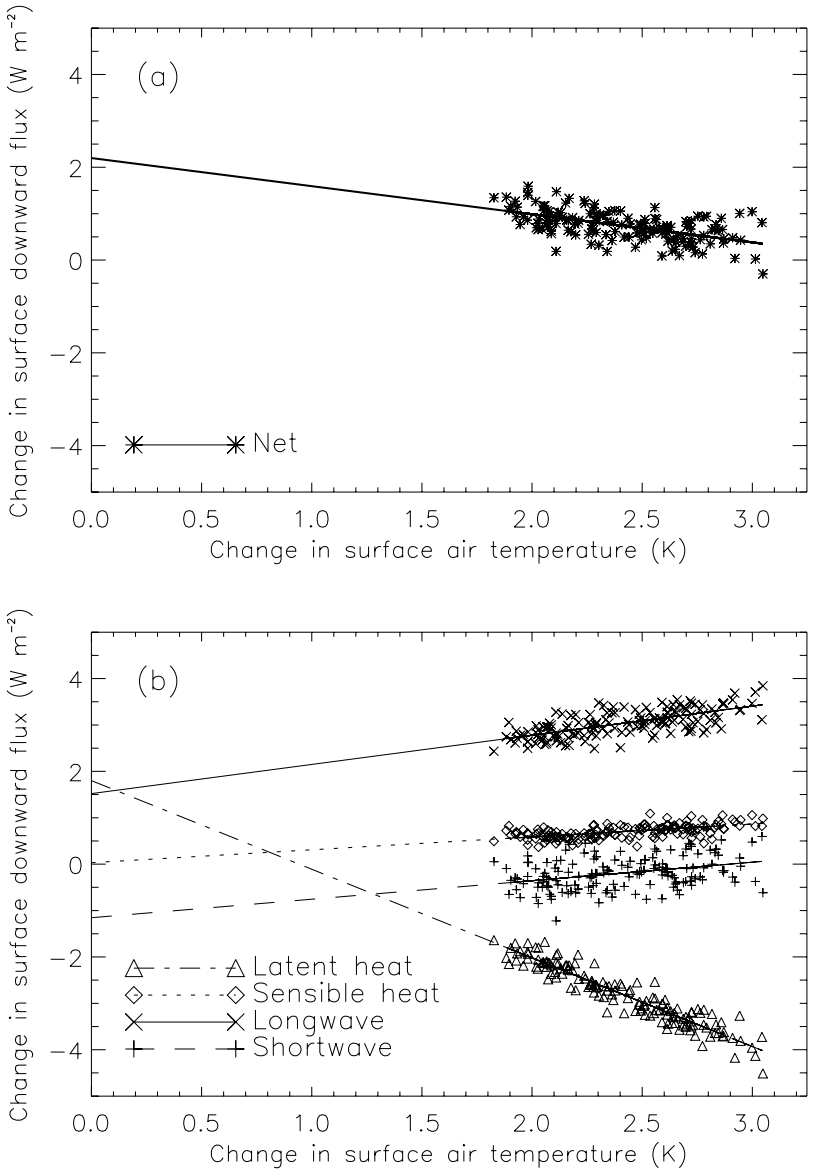

Figure 2. (a) Regression of change in global mean net surface energy flux, N, against change in global mean surface air temperature, ΔT, after the 70th year in the UKMO-HadGEM1 1% yr^{-1} CO_2 increase until 2 × CO_2 is reached experiment. (b) Same as Figure 2a but for the surface energy components, N_i. Symbols are annual means, and the lines are the regressions. All fluxes are defined as positive downward.

coupled to a fully dynamic ocean and slab ocean (Table 2), though the net feedback is in reasonable agreement. The differences are not unexpected and support earlier studies that suggest a fully dynamic ocean can modify atmospheric feedbacks [e.g., *Boer and Yu*, 2003a].

[18] Some studies suggest that α_i may be somewhat dependent on climate state [e.g., *Senior and Mitchell*, 2000; *Boer and Yu*, 2003b; *Yokohata et al.*, 2008]. In the following analysis it is assumed that α_i is independent of climate state, and so α_i is constant in time. Recent work

Table 2. Components of the Global Mean Surface Climate Feedback Parameter Diagnosed From the 1% yr^{-1} CO_2 Increase Until 2 × CO_2 is Reached Experiment[a]

	Y_{LW}	Y_{SW}	Y_{LH}	Y_{SH}	Y_{Net}
UKMO-HadGEM1	0.63 ± 0.06	0.40 ± 0.09	−1.91 ± 0.05	0.28 ± 0.03	−0.61 ± 0.07
UKMO-HadGEM1 (Slab)	0.91 ± 0.06	0.21 ± 0.08	−2.22 ± 0.02	0.43 ± 0.04	−0.67 ± 0.09

[a]Units: W m^{-2} K^{-1}. Values represent the gradient of the regression lines in Figures 2a and 2b with corresponding 1−σ uncertainties. Also shown for comparison are the values determined by *Andrews et al.* [2009] for UKMO-HadGEM1 coupled to a slab ocean forced by an instantaneous doubling of CO_2.

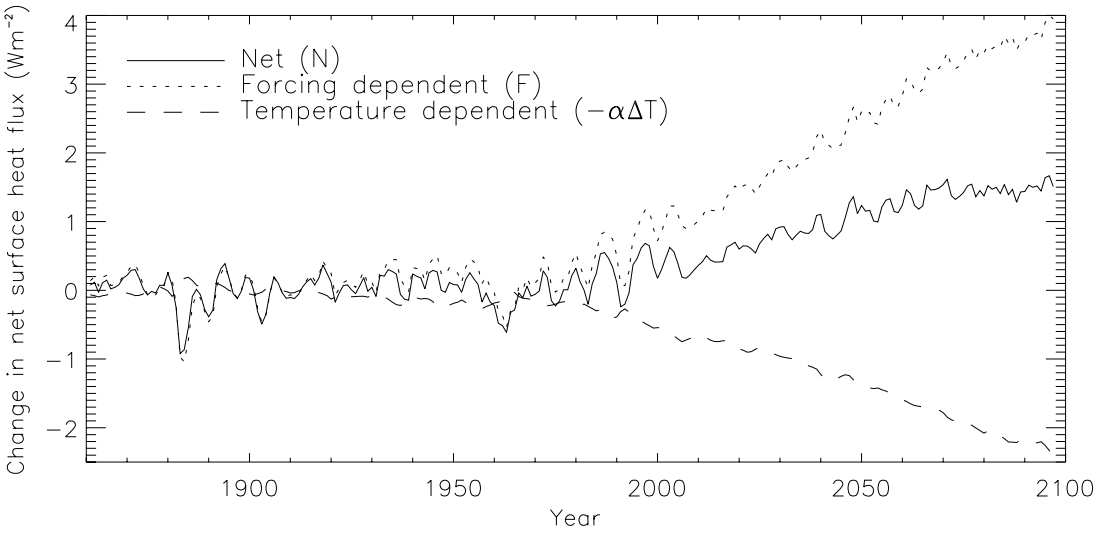

Figure 3. UKMO-HadGEM1 simulated time series of the 20th century and A1B scenario net surface energy imbalance N (solid line) and its separation into forcing F (dotted line) and response $-\alpha\Delta T$ (dashed line). A 3-year boxcar smoothing has been applied. Fluxes are defined as positive downward.

supports such an assumption; for example, *Williams et al.* [2008] showed that the apparent time variation of the effective climate sensitivity (or equivalently the climate feedback parameter) is in fact due to forcing definitions that exclude any rapid tropospheric adjustments. If one includes these adjustments in the forcing, as is done in this study, then the effective climate sensitivity shows little time variation [*Williams et al.*, 2008]. As in the work by *Forster and Taylor* [2006], one further assumption must also be made, namely that the diagnosed feedback parameters are forcing-independent, and so they can be applied to any forcing scenario.

3.2. Separated Surface Energy Trends

[19] Given α_i (Table 2) it is now possible to determine the global mean 20th century and SRES A1B F_i time series from equation (1), therefore separating forcing-dependent changes (F_i) from climate feedbacks ($\alpha_i\Delta T$) under the assumption that the α_i terms are independent of the forcing scenario.

[20] Figure 3 shows the 20th century and SRES A1B 21st century time series of the net surface energy imbalance (solid line), N, and how this is separated into surface forcing (dotted line), F, and climate response (dashed line), $-\alpha\Delta T$, according to equation (1). Positive downward surface forcing slowly increases over the 20th century (Figure 3, dotted line), to nearly 1 W m^{-2} by 1999. This trend continues into the A1B scenario, reaching a maximum surface forcing of nearly 4 W m^{-2} by the end of the 21st century. There exists significant noise in the 20th century forcing time series, though some of the largest negative spikes can be associated with volcanic eruptions (see further below). Climate response (dashed line) acts to oppose F, which it must for a stable system. Owing to the large heat capacity of the Earth's oceans (which determines the rate of climate response) F and $-\alpha\Delta T$ do not cancel, so the Earth's net surface energy imbalance (solid line) is generally positive, rising to ~1.5 W m^{-2} by the end of the 21st century under the A1B scenario (Fi and Table 1). This finding supports the idea that even if climate forcings were to be held constant the climate would continue to respond to the remaining imbalance [e.g., *Hansen et al.*, 2005a].

[21] Net forcing and response is separated into component form in Figure 4. Net surface LW (N_{LW}) increases with time, mostly composed of LW forcing (F_{LW}) but there is a small contribution from feedback ($Y_{LW}\Delta T$), which gets increasingly important during the A1B projected 21st century (Figure 4a). The forcing component is most likely the result of increases in GHGs, which will immediately increase LW down at the surface; UKMO-HadGEM1 indicates this to be ~1.6 W m^{-2} by the late 20th century (Table 1). The smaller contribution from feedback is associated with water-vapor and cloud feedback, as well as the atmosphere increasing its thermal emission at it warms. The sum of these feedbacks leads to an increase in LW radiation at the surface and outweighs the opposing thermal surface response, so leading to a positive LW surface feedback [e.g., *Ramanathan*, 1981; *Allan*, 2006; *Andrews et al.*, 2009], seen also in Table 2. At the end of the 21st century the contribution from forcing to the increase in net surface LW radiation is nearly double the contribution from feedback. Stabilizing atmospheric levels of GHGs in the future would stabilize the surface LW forcing, though the contribution from feedback would continue to rise as ΔT increased.

[22] The temperature-dependent component of net surface SW ($Y_{SW}\Delta T$) increases over the entire time period (Figure 4b), so that as ΔT positively increases over time more SW radiation is absorbed by the Earth's surface. This is the net effect of complicated and uncertain processes involving water vapor, surface albedo and clouds, all of which can change in response to ΔT and impact the SW radiation budget. This is not, however, the main driver of the surface SW radiation budget; surface SW forcings (F_{SW}) are significantly larger than response (Figure 4b and Table 1). Over the 20th and most of the 21st centuries surface SW forcing is increasingly large and negative (Figure 4b), consistent with an increasing burden of

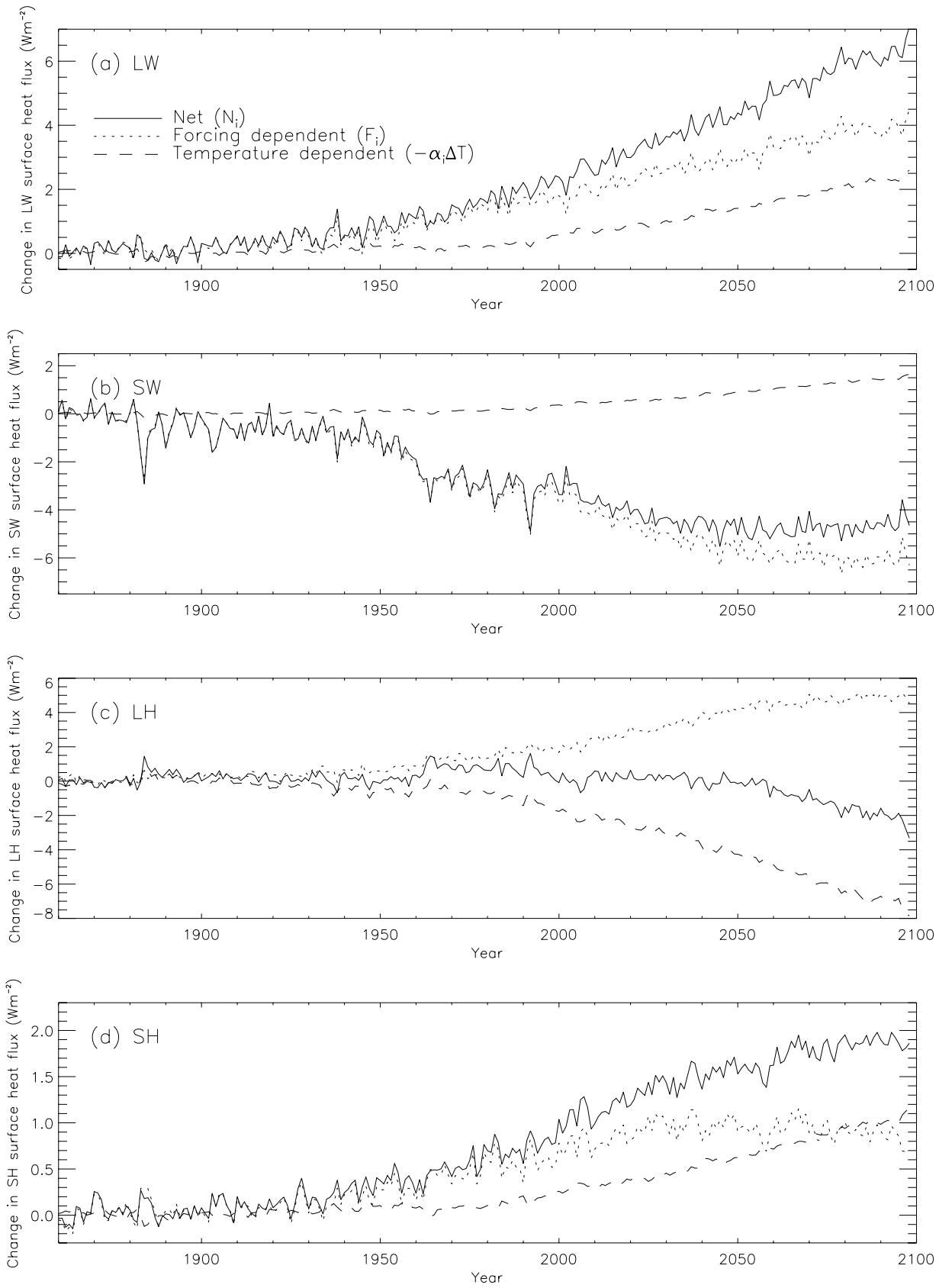

Figure 4. Same as Figure 3 but for the surface energy budget components. (a) LW, (b) SW, (c) LH, and (d) SH. All fluxes are defined as positive downward. No smoothing has been applied.

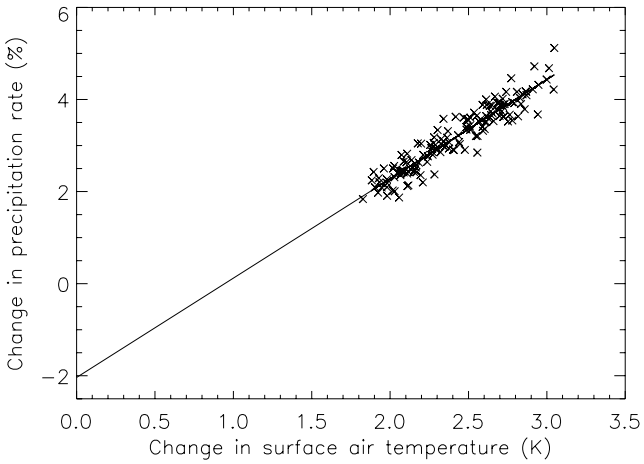

Figure 5. Regression of change in global precipitation rate against ΔT after the 70th year in the UKMO-HadGEM1 1% yr^{-1} CO_2 increase until 2 × CO_2 is reached experiment. Symbols are annual means, and the line is the regression.

atmospheric aerosols which generate negative surface forcings due to the scattering and absorbing of solar radiation [*Forster et al.*, 2007]. The reduction in SW radiation at the Earth's surface over the 20th century is consistent with other models [see *Romanou et al.*, 2007]. Twentieth century SW surface forcings are also interrupted by large, but short-lived, negative spikes (Figure 4b) that coincide with large volcanic eruptions, for example, Krakatoa (1883), Agung (1963), El Chichon (1982) and Pinatubo (1991). Volcanic eruptions inject sulfate aerosols into the stratosphere and so directly reduce SW radiation at the surface, as seen in Figure 4b. The SW forcing trend will also be affected by rapid cloud responses to forcing agents, such as the indirect and semidirect effect of aerosols, and any analogous cloud responses to CO_2 or other GHGs [*Gregory and Webb*, 2008; *Andrews and Forster*, 2008; *Williams et al.*, 2008].

[23] Changes in the surface radiation budget relating to climate feedback are similar between LW and SW radiation (see Figures 4a and 4b and Table 2), both of which increase with positive ΔT. In contrast the LW and SW surface forcing oppose each other (Table 1), but the larger in magnitude SW forcing leads to a generally negative radiative component of surface forcing (~ -1.7 W m^{-2} averaged over the last 25 years of the 20th century). This estimate of the late 20th century surface radiative forcing is in general agreement with other recent estimates [e.g., *Forster et al.*, 2007, Figure 2.23], which attributed the strong negativity to the presence of aerosols, despite the differences in forcing definitions (the definition used by *Forster et al.* [2007] did not include any tropospheric adjustment).

[24] The Earth's surface loses the excess energy gain from radiative feedbacks (LW and SW response) by increasing its evaporative cooling, indicated by an increasingly negative LH flux with ΔT (Figure 4c, dashed line). Opposing this large LH flux change is a forcing dependence which acts to suppress the LH flux increase to the atmosphere. For example, at the end of the 21st century the surface LH flux to the atmosphere increases by $\sim$7.5 W m^{-2} according to ΔT; however, this is suppressed by an induced LH forcing component, leading to $\sim$2 W m^{-2} change in the net LH flux (Figure 4c). Previous studies found that the LH flux rapidly reduces its flux to the atmosphere in response to increased CO_2 levels (and most probably any forcing that is strongly absorbed in the troposphere such as other GHG forcings) in order to restore the tropospheric heat budget [e.g., *Mitchell*, 1983; *Mitchell et al.*, 1987; *Allen and Ingram*, 2002; *Yang et al.*, 2003; *Lambert and Faull*, 2007; *Andrews et al.*, 2009]. Under this analysis such an adjustment is included in the forcing, and so these previous studies support the results found here.

[25] There is a small positive response of the SH flux to ΔT, but most of its changes are forcing-dependent during the 20th century (Figure 4d). SH forcing saturates during the 21st century and follows a similar trend to that of SW surface forcing. It is possible that the SH forcing is induced by forcing mechanisms that strongly affect the SW radiation budget, such as aerosols, but a more rigorous explanation would require further work, beyond the scope of this paper.

[26] The net turbulent surface forcing (e.g., $F_{LH} + F_{SH} \sim$ 2.5 W m^{-2} (6 W m^{-2}) at the end of the 20th (21st) century) is larger than the net radiative surface forcing (e.g., $F_{LW} + F_{SW} \sim -1.5$ W m^{-2} (-2 W m^{-2}) at the end of the 20th (21st) century), and so leads to a generally positive net surface forcing trend over the 20th and 21st centuries (Figure 3).

4. Global Hydrological Cycle

[27] On monthly or longer time scales, global evaporation balances global precipitation. Given that the surface LH flux exhibits both significant forcing and temperature-dependent changes (see section 3) this should also impact precipitation trends.

4.1. Separation of Precipitation Trends

[28] In analogy to section 3, one can determine how global precipitation, P, responds to ΔT by regressing change in global precipitation, ΔP, against ΔT after 70 years in the 1% yr^{-1} CO_2 increase experiment, shown in Figure 5. The % change in precipitation rate per ΔT, referred to as the "differential hydrological sensitivity" [*Andrews et al.*, 2009], is determined from the gradient of the regression line (Figure 5). In this case it is 2.16 ± 0.06% K^{-1}, which is within the range (1.4–3.4% K^{-1}) determined by *Lambert and Webb* [2008], who investigated the dependence of P on ΔT in other models using a similar regression method. Note that the "differential hydrological sensitivity" is different from the hydrological sensitivity because the latter is usually determined from equilibrium and therefore does not separate the forcing-dependent adjustment to precipitation rate from the response to ΔT [*Lambert and Webb*, 2008; *Andrews et al.*, 2009].

[29] The differential hydrological sensitivity can then be used to separate forcing-dependent precipitation adjustments from its response to ΔT in the 20th century and A1B trends, in an analogous way to how the surface energy trends were separated using equation (1). As for the surface energy budget, one must assume that the differential hydrological sensitivity is independent of the forcing agent, so it can be applied to different forcing scenarios; both *Lambert and Faull* [2007] and *Andrews et al.* [2009] showed that it is similar between a CO_2 and solar increase experiment.

Table 3. Change in Global Mean Surface Energy Fluxes Averaged Over the Last 25 Years of the 20th Century Simulation Compared to the Pre-industrial Control State for Various AOGCMs Participating in CMIP3[a]

	LW	SW	LH	SH	Net
CGCM3.1(T47)	1.38	−0.10	−1.18	0.42	0.53
GFDL-CM2.0	1.70	−2.82	0.73	0.66	0.27
GISS-AOM	0.92	−0.74	−0.41	0.78	0.56
INM-CM3.0	1.25	−0.68	−0.61	0.50	0.46
IPSL-CM4	1.65	−0.44	−0.90	0.33	0.63
MRI-CGCM2.3.2	1.21	−0.76	−0.90	0.87	0.43
UKMO-HadCM3	1.42	−0.82	−0.37	0.15	0.38
UKMO-HadGEM1	1.89	−3.10	0.70	0.71	0.20
AOGCM-mean	1.43	−1.18	−0.37	0.55	0.43
AOGCM-StdDev	0.31	1.12	0.72	0.25	0.15

[a]Units: W m^{-2}; years: 1975–1999. All fluxes are defined as positive downward.

Results reveal (not shown) a mirror image of the surface latent heat flux (shown in Figure 4c), as global precipitation is very well correlated with global evaporation in this model. Precipitation therefore can be directly influenced by forcing agents independent of global temperature change. For example in response to ΔT global precipitation rate increases by ∼8% by the end of the A1B 21st century. However, the realized precipitation increase is ∼2.5% because climate forcing agents directly reduce global precipitation rate by ∼5.5%.

4.2. Discussion on Observed Precipitation Changes

[30] Recent observational studies [e.g., *Wentz et al.*, 2007; *Yu and Weller*, 2007; *Allan and Soden*, 2007] suggest that GCMs underestimate the precipitation response to global temperature change. For example, per degree of warming current GCMs simulate an increased precipitation response of ∼1.4–3.4% K^{-1} [*Lambert and Webb*, 2008]. *Wentz et al.* [2007] used satellite observations to show that real world precipitation responds to global temperature increases by ∼7% K^{-1}, much larger than the model response and close to the expectations of the Clausius-Clapeyron relation. *Wentz et al.* [2007] assumed constant near-surface relative humidity and air-sea temperature difference, and so attributed the models muted precipitation response to an unrealistic decrease in global winds. However, these assumptions need further validation. For example, *Richter and Xie* [2008] showed that surface relative humidity and surface stability robustly increased across models, both of which would dampen evaporation and hence reduce precipitation.

[31] *Wentz et al.* [2007] interpreted the discrepancy between models and observations as an erroneous model response to global warming. However, this remains to be proven. *Adler et al.* [2008] used a longer observing time period and determined a precipitation response to warming similar to that of the models, but their results were sensitive to the time period considered. Furthermore, these interpretations of observations implicitly assumed that the precipitation changes were due to changes in global temperature, neglecting the direct effect of forcing agents on precipitation [*Lambert et al.*, 2008].

[32] Diagnosed precipitation response to warming from observations (by simply comparing the observed change in precipitation to the observed change in temperature) is equivalent to using the net change in precipitation rate (i.e., not separating the response to global temperature change from the direct influence of forcing agents, analogous to the solid line in Figure 4c for the surface latent heat flux). Arbitrarily choosing a time period, say that observed by *Adler et al.* [2008] (1979–2006), UKMO-HadGEM1 simulates a net precipitation increase of 0.44% $decade^{-1}$ and a global mean surface temperature increase of 0.31 K $decade^{-1}$, determined from linear trends of annual global means over the considered time period. Hence this suggests a precipitation sensitivity of ∼1.42% K^{-1}, which is smaller than the "true" value of 2.16% K^{-1} for this model diagnosed in section 4.1 (note that this comparison neglects natural variability, which would be a significant source of uncertainty [see *Previdi and Liepert*, 2008]). If climate forcing agents are directly suppressing precipitation in the real world, then current observations may underestimate the true response of precipitation to global warming. However, caution is urged in inferring that this result implies the gap between model and observed precipitation response to global warming should be larger, for the following reasons: (1) this result depends crucially on the assumption that the diagnosed differential hydrological sensitivity from the CO_2 experiment can be applied to other forcing simulations where many other forcing agents are present, and (2) current observations need further validation and may not represent the long-term response, for example, models can produce large sensitivity values on short time periods that are consistent with current observations due to natural variability [*Previdi and Liepert*, 2008]. Nevertheless, past observational studies have not considered the direct impact forcing mechanisms may have on precipitation.

5. Intercomparison of Models

[33] While the focus of this paper was to illustrate the method and analyze the results of one model in detail it is useful to compare changes in the surface energy balance of other models. Table 3 shows the net change (i.e., N_i components) in surface energy terms at the end of the 20th century (averaged over 1975–1999) compared to the pre-industrial control state for various AOGCMs participating in CMIP3. There is good agreement across the models for the net surface energy imbalance N, AOGCM average equals 0.43 ± 0.15 W m^{-2}, with UKMO-HadGEM1 having the smallest value (N = 0.2 W m^{-2}) while L'Institut Pierre-Simon Laplace Coupled Model version 4 (IPSL-CM4) has the largest value (N = 0.63 W m^{-2}). As most of this imbalance will be taken up by the oceans these model results support an observed increase in ocean heat content and a warming of the world ocean [e.g., *Levitus et al.*, 2005].

[34] There is less agreement in how the surface energy imbalance is partitioned between the LW, SW, LH and SH fluxes (Table 3). While all the models show a reduction in SW radiation at the surface, there is considerable uncertainty in its magnitude. For example the Canadian Centre for Climate Modeling and Analysis (CCCma) Coupled General Circulation Model version 3.1 at resolution T47 (CGCM3.1(T47)) shows a modest reduction of only 0.1 W m^{-2} whereas the Geophysical Fluid Dynamics Laboratory Coupled Model version 2.0 (GFDL-CM2.0) and UKMO-HadGEM1 exhibit

reductions of 2.82 W m^{-2} and 3.10 W m^{-2}, respectively. The spread in absorbed SW radiation at the surface has a significant impact on the robustness of the hydrological response. For most models there is an increase in LW radiation and SH flux at the surface that is larger than the reduced SW radiation, and so a decrease in positive downward LH flux (i.e., an increase in LH flux to the atmosphere and an intensified hydrological cycle). The strength of this change is constrained by the amount of energy available at the surface. For GFDL-CM2.0 and UKMO-HadGEM1 the decrease in SW radiation is so large (larger than the compensating change in LW radiation and SH flux) that less energy is available for the hydrological cycle than in the pre-industrial control state; hence in these models the LH flux to atmosphere is actually reduced.

[35] *Andrews et al.* [2009] examined the surface feedbacks of slab-ocean versions of various models participating in CMIP3 and found some spread across models. It is likely that a similar spread exists among the fully coupled models and so could explain some of the differences found in Table 3. On the other hand, *Forster and Taylor* [2006] found a significant spread across model TOA forcing, and so a spread across model surface forcing also likely contributes to these differences. A spread in model forcing could have several sources: (1) different forcings mechanisms applied to the model, for example, some models include volcanic aerosols and some do not [e.g., see *Forster and Taylor*, 2006], (2) differences in the radiative forcing calculation for well-mixed GHGs or other mechanisms [e.g., *Collins et al.*, 2006; *Forster and Taylor*, 2006], and (3) differences in the fast responses, i.e., tropospheric adjustments, which are included as part of the forcing in this analysis and have been shown to be uncertain across models [*Gregory and Webb*, 2008; *Andrews and Forster*, 2008; *Andrews et al.*, 2009].

[36] Understanding the way the surface energy imbalance is partitioned between the LW, SW, LH and SH fluxes presented in Table 3 would be useful. In particular, as the magnitude of the reduction in SW radiation absorbed at the surface is important for determining the sign of the hydrological response, it would be useful to examine whether forcings or feedbacks in models are responsible for the spread in SW radiation at the surface. This analysis would require other model diagnostics such as those employed for the UKMO-HadGEM1 model in section 3.

6. Conclusions

[37] A simple methodology has been applied to a transient integration of the UKMO-HadGEM1 fully coupled AOGCM in order to separate forcing-dependent changes from climate response in simulated 20th century and A1B scenario 21st century surface energy and precipitation trends. Results show that over the 20th and 21st centuries surface radiative forcing is dominated by SW forcings, which are strongly negative and consistent with increased aerosol load. Large, but short-lived, negative SW forcing signals due to simulated volcanic eruptions are found in the 20th century simulation (the 21st century scenario did not include volcanic forcings). Surface radiative forcing is considerably larger than the influence of climate feedbacks on the surface radiation budget.

[38] Despite a negative surface radiative forcing, 20th and 21st century net surface forcing is positive when rapid surface and tropospheric adjustments are included in the forcing. This is because both the latent and sensible heat fluxes respond directly to climate forcing agents, independent of global temperature change. Accounting for the latent heat surface forcing is important for correctly understanding past and future trends in evaporation and precipitation. For example by the end of the A1B 21st century global precipitation rate increases by ~8% in response to global temperature change, compared to the pre-industrial control state. However, the realized precipitation increase is only ~2.5% because climate forcing agents directly suppress precipitation by ~5.5%. Recent observations of the global precipitation response to global warming have not accounted for the direct influence forcing agents may have on precipitation.

[39] An intercomparison of climate models reveals that the Earth's surface is out of energy balance (AOGCM average equals 0.43 ± 0.15 W m^{-2}) by the late 20th century. However, there is considerable disagreement in how this imbalance is partitioned between the longwave, shortwave, sensible and latent heat fluxes. For example all models show reductions in the amount of shortwave radiation absorbed at the surface, but there exists a large spread in the magnitude of this reduction. In particular, for some models the reduction is large enough to outweigh the energy gain from changes in both surface longwave and sensible heat fluxes, leading to less energy available to evaporate surface water and leading to a reduced intensity of the hydrological cycle. In future work it would be useful to identify why models disagree in how the surface energy imbalance is partitioned.

[40] **Acknowledgments.** I am grateful to Piers Forster for invaluable input to this work, Olivier Boucher for providing useful comments on an earlier draft, and three anonymous reviewers for their constructive comments. I also acknowledge the modeling groups, the Program for Climate Model Diagnosis and Intercomparison (PCMDI) and the WCRP's Working Group on Coupled Modeling (WGCM), for their roles in making available the WCRP CMIP3 multimodel data set. Support of this data set is provided by the Office of Science, U.S. Department of Energy. This work was funded by a NERC open CASE award with the UK Met Office.

References

Adler, R. F., G. Gu, J.-J. Wang, G. J. Huffman, S. Curtis, and D. Bolvin (2008), Relationships between global precipitation and surface temperature on interannual and longer timescales (1979–2006), *J. Geophys. Res.*, *113*, D22104, doi:10.1029/2008JD010536.

Allan, R. P. (2006), Variability in clear-sky longwave radiative cooling of the atmosphere, *J. Geophys. Res.*, *111*, D22105, doi:10.1029/2006JD007304.

Allan, R. P., and B. J. Soden (2007), Large discrepancy between observed and simulated precipitation trends in the ascending and descending branches of the tropical circulation, *Geophys. Res. Lett.*, *34*, L18705, doi:10.1029/2007GL031460.

Allen, M. R., and W. J. Ingram (2002), Constraints on future changes in climate and the hydrological cycle, *Nature*, *419*, 224–232, doi:10.1038/nature01092.

Andrews, T., and P. M. Forster (2008), CO_2 forcing induces semi-direct effects with consequences for climate feedback interpretations, *Geophys. Res. Lett.*, *35*, L04802, doi:10.1029/2007GL032273.

Andrews, T., P. M. Forster, and J. M. Gregory (2009), A surface energy perspective on climate change, *J. Clim.*, *22*, 2557–2570, doi:10.1175/2008JCLI2759.1.

Boer, G. J. (1993), Climate change and the regulation of the surface moisture and energy budgets, *Clim. Dyn.*, *8*, 225–239, doi:10.1007/BF00198617.

Boer, G. J., and B. Yu (2003a), Dynamical aspects of climate sensitivity, *Geophys. Res. Lett.*, *30*(3), 1135, doi:10.1029/2002GL016549.

Boer, G. J., and B. Yu (2003b), Climate sensitivity and climate state, *Clim. Dyn.*, *21*, 167–176, doi:10.1007/s00382-003-0323-7.

Collins, W. D., et al. (2006), Radiative forcing by well-mixed greenhouse gases: Estimates from climate models in the IPCC AR4, *J. Geophys. Res.*, *111*, D14317, doi:10.1029/2005JD006713.

Forster, P. M., and K. E. Taylor (2006), Climate forcings and climate sensitivities diagnosed from coupled climate model integrations, *J. Clim.*, *19*, 6181–6194, doi:10.1175/JCLI3974.1.

Forster, P., et al. (2007), Changes in atmospheric constituents and in radiative forcing, in *Climate Change 2007: The Physical Science Basis. Contribution of Working Group 1 to the Fourth Assessment Report of the Intergovernmental Panel on Climate Change*, edited by S. Solomon et al., pp. 131–234, Cambridge Univ. Press, Cambridge, U. K.

Gregory, J. M., and M. Webb (2008), Tropospheric adjustment induces a cloud component in CO_2 forcing, *J. Clim.*, *21*, 58–71, doi:10.1175/2007JCLI1834.1.

Gregory, J. M., W. J. Ingram, M. A. Palmer, G. S. Jones, P. A. Stott, R. B. Thorpe, J. A. Lowe, T. C. Johns, and K. D. Williams (2004), A new method for diagnosing radiative forcing and climate sensitivity, *Geophys. Res. Lett.*, *31*, L03205, doi:10.1029/2003GL018747.

Hansen, J., et al. (2005a), Earth's energy imbalance: Confirmation and implications, *Science*, *308*, 1431–1435, doi:10.1126/science.1110252.

Hansen, J., et al. (2005b), Efficacy of climate forcings, *J. Geophys. Res.*, *110*, D18104, doi:10.1029/2005JD005776.

Held, I. M., and B. J. Soden (2006), Robust responses of the hydrological cycle to global warming, *J. Clim.*, *19*, 5686–5699, doi:10.1175/JCLI3990.1.

Lambert, F. H., and N. E. Faull (2007), Tropospheric adjustment: The response of two general circulation models to a change in insolation, *Geophys. Res. Lett.*, *34*, L03701, doi:10.1029/2006GL028124.

Lambert, F. H., and M. J. Webb (2008), Dependence of global mean precipitation on surface temperature, *Geophys. Res. Lett.*, *35*, L16706, doi:10.1029/2008GL034838.

Lambert, F. H., A. R. Stine, N. Y. Krakauer, and J. C. H. Chiang (2008), How much will precipitation increase with global warming?, *Eos Trans. AGU*, *89*(21), doi:10.1029/2008EO210001.

Levitus, S., J. Antonov, and T. Boyer (2005), Warming of the world ocean, 1955–2003, *Geophys. Res. Lett.*, *32*, L02604, doi:10.1029/2004GL021592.

Meehl, G. A., et al. (2007), Global climate projections, in *Climate Change 2007: The Physical Science Basis. Contribution of Working Group 1 to the Fourth Assessment Report of the Intergovernmental Panel on Climate Change*, edited by S. Solomon et al., pp. 591–662, Cambridge Univ. Press, Cambridge, U. K.

Mitchell, J. F. B. (1983), The seasonal response of a general circulation model to changes in CO_2 and sea temperatures, *Q. J. R. Meteorol. Soc.*, *109*, 113–152.

Mitchell, J. F. B., C. A. Wilson, and W. M. Cunnington (1987), On CO_2 climate sensitivity and model dependence of results, *Q. J. R. Meteorol. Soc.*, *113*, 293–322, doi:10.1256/smsqj.47516.

Nakicenovic, N., , and R. Swart (Eds.) (2000), *Special Report on Emission Scenarios*, Cambridge Univ. Press, Cambridge, U. K.

National Research Council (2005), *Radiative Forcing of Climate Change*, 207 pp., Natl. Acad. Press, Washington, D. C.

Pielke, R. A. (2003), Heat storage within the earth system, *Bull. Am. Meteorol. Soc.*, *84*, 331–335, doi:10.1175/BAMS-84-3-331.

Previdi, M., and B. Liepert (2008), Interdecadal variability of rainfall on a warming planet, *Eos Trans. AGU*, *89*(21), doi:10.1029/2008EO210002.

Ramanathan, V. (1981), The role of ocean-atmosphere interactions in the CO_2 climate problem, *J. Clim.*, *38*, 918–930.

Randall, D. A., et al. (2007), Climate models and their evaluation, in *Climate Change 2007: The Physical Science Basis. Contribution of Working Group 1 to the Fourth Assessment Report of the Intergovernmental Panel on Climate Change*, edited by S. Solomon et al., pp. 591–662, Cambridge Univ. Press, Cambridge, U. K.

Richter, I., and S. P. Xie (2008), The muted precipitation increase in global warming simulations: A surface evaporation perspective, *J. Geophys. Res.*, *113*, D24118, doi:10.1029/2008JD010561.

Romanou, A., B. Liepert, G. A. Schmidt, W. B. Rossow, R. A. Ruedy, and Y. Zhang (2007), 20th century changes in surface solar irradiance in simulations and observations, *Geophys. Res. Lett.*, *34*, L05713, doi:10.1029/2006GL028356.

Senior, C. A., and J. F. B. Mitchell (2000), The time-dependence of climate sensitivity, *Geophys. Res. Lett.*, *27*(17), 2685–2688, doi:10.1029/2000GL011373.

Shine, K. P., J. Cook, E. J. Highwood, and M. M. Joshi (2003), An alternative to radiative forcing for estimating the relative importance of climate change mechanisms, *Geophys. Res. Lett.*, *30*(20), 2047, doi:10.1029/2003GL018141.

Soden, B. J., A. J. Broccoli, and R. S. Hemler (2004), On the use of cloud forcing to estimate cloud feedback, *J. Clim.*, *17*, 3661–3665, doi:10.1175/1520-0442(2004)017<3661:OTUOCF>2.0.CO;2.

Soden, B. J., I. M. Held, R. Colman, K. M. Shell, J. T. Kiehl, and C. A. Shields (2008), Quantifying climate feedbacks using radiative kernels, *J. Clim.*, *21*, 3504–3520, doi:10.1175/2007JCLI2110.1.

Stott, P. A., G. S. Jones, J. A. Lowe, P. Thorne, C. Durman, T. C. Johns, and J. C. Thelen (2006), Transient climate simulations with the HadGEM1 climate model: Causes of past warming and future climate change, *J. Clim.*, *19*, 2763–2782, doi:10.1175/JCLI3731.1.

Wentz, F. J., L. Ricciardulli, K. Hilburn, and C. Mears (2007), How much more rain will global warming bring?, *Science*, *317*, 233–235, doi:10.1126/science.1140746.

Wild, M., J. Grieser, and C. Schär (2008), Combined surface solar brightening and increasing greenhouse effect support recent intensification of the global land-based hydrological cycle, *Geophys. Res. Lett.*, *35*, L17706, doi:10.1029/2008GL034842.

Williams, K. D., W. J. Ingram, and J. M. Gregory (2008), Time variation of effective climate sensitivity in GCMs, *J. Clim.*, *21*, 5076–5090, doi:10.1175/2008JCLI2371.1.

Yang, F., A. Kumar, M. E. Schlesinger, and W. Wang (2003), Intensity of hydrological cycles in warmer climates, *J. Clim.*, *16*, 2419–2423, doi:10.1175/2779.1.

Yokohata, T., et al. (2008), Comparison of equilibrium and transient responses to CO_2 increases in eight state-of-the-art climate models, *Tellus, Ser. A*, *60*, 946–961, doi:10.1111/j.1600-0870.2008.00345.x.

Yu, L., and R. A. Weller (2007), Objectively analyzed air-sea heat fluxes for the global ice-free oceans (1981–2005), *Bull. Am. Meteorol. Soc.*, *88*, 527–539, doi:10.1175/BAMS-88-4-527.

Zhang, Y., W. B. Rossow, P. Stackhouse Jr., A. Romanou, and B. A. Wielicki (2007), Decadal variations of global energy and ocean heat budget and meridional energy transports inferred from recent global data sets, *J. Geophys. Res.*, *112*, D22101, doi:10.1029/2007JD008435.

T. Andrews, School of Earth and Environment, University of Leeds, Leeds LS2 9JT, UK. (t.andrews@see.leeds.ac.uk)